Materials Research Express

ACCEPTED MANUSCRIPT

Effect of cation ratio on microstructure and optical absorbance of magnesium aluminate spinel

To cite this article before publication: Rupa Halder *et al* 2019 *Mater. Res. Express* in press https://doi.org/10.1088/2053-1591/ab5f8b

Effect of cation ratio on microstructure and optical absorbance of magnesium aluminate spinel

R. Halder, S. Bandyopadhyay*

CSIR- Central Glass & Ceramic Research Institute

196, Raja S.C. Mullick Road, Kolkata 700 032, India

Abstract

This work is pertaining to the synthesis of fine magnesium aluminate spinel ($MgAl_2O_4$) powders of varied trivalent:bivalent cation ratio along line of homogeneity of the solid solution (MgO. xAl_2O_3, x=1, 1.25, 1.50, 1.75, and 2) via gel combustion method. Magnesium- and aluminum- nitrate were used as the oxidants in combustion reaction fuelled by urea in combination with stoichiometric formaldehyde solution acting as reductant. Synthesized powders were characterized in terms of microscopic analysis and optical absorbance measurements. The cation ratio, through a change in gel structure influences the nature of crystallization of the product, while on the other hand does not affect grain shapes and sizes. Distinct enhancement in both absorption intensity and the corresponding estimated energy band gap has been observed against increasing excess than stiochiometric alumina concentrations. Evaluated optical band gaps were widened in proportion to the Al: Mg ratio which may be attributed to Burstein-Moss effect in consequence of substitutional insertion of introduced Al^{3+} ions in spinel lattices.

Keywords: Magnesium aluminate spinel; Cation ratio; Gel combustion; Band gap.

*Corresponding author, sbando@cgcri.res.in, +91 33 2322 3475

1. Introduction

Studies on the stability of the spinel structured materials under high pressure, viz., pressure dependent phase transition in $ZnAl_2O_4$ and $ZnGa_2O_4$ have been performed in several works [1,2]. Room-temperature angle-dispersive x-ray diffraction measurements on spinel $ZnGa_2O_4$ upto 56 GPa shows two structural phase transition; one, at 31.2 GPa where $ZnGa_2O_4$ undergoes a transition from the cubic spinel structure to a tetragonal spinel structure and the other at 55 GPa where transition to the orthorhombic marokite structure ($CaMn_2O_4$-type) takes place. Similarly, ab-initio study [3] on the high pressure polymorphism of $MgAl_2O_4$ reveals the equilibrium pressures for the reactions of formation/decomposition of the low pressure stable-*Fd3m* to high pressure stable-*Cmcm* type polymorphs to be ranging in the pressure of 0 to 60 GPa. According to the density functional theory through LDA & B3LYP calculations, this polymorph transformation takes place at 39 and 57 GPa, respectively. Owing to some excellent features of this stable $MgAl_2O_4$ under ambient pressure like high melting point (2135^{o}C), low thermal conductivity, good thermal shock resistance, chemical inertness, and good mechanical strength both at room temperature as well as high temperature, magnesium aluminate spinel ($MgAl_2O_4$) has been used as refractory materials in steel ladles, vacuum induction furnaces [4] etc. It is also ideal for use as insulating material [5], optical material [6], humidity sensors [7], and photocatalyst activity [8]. Recent attraction of this material is for its use as transparent window applications [9] in high performance sectors. There are several wet-chemical processes those are currently used for the production of spinel powder at low temperature and low cost, such as sol-gel [10], Pechini [11], co-precipitation [12], spray drying [13], freeze drying [14] etc. Gel combustion method [15] is a self propagating exothermic reaction route where the gel burst into smaller units and simultaneously disintegrates into fine powder.

In this paper, we have aimed to prepare nanoscale magnesium aluminate spinel with stoichiometric composition of magnesia (MgO) to alumina (Al_2O_3) as well as of different alumina-richer compositions through gel combustion method. Influence of larger trivalent to divalent cation content on the synthesis and optical property (viz. absorbance and band gap) of all gel combusted powders was investigated.

2. Experimental procedure

2.1. Materials and methods-

Aluminium nitrate nonahydrate, [$Al(NO_3)_3{\cdot}9H_2O$], magnesium nitrate hexahydrate [$Mg(NO_3)_2{\cdot}6H_2O$], urea (Merck, India), formaldehyde solution [37% (w/v), Merck, India], nitric acid (Merck, India) and ammonia solution (Merck, India), all of LR grade were used as starting reagents. Methylol urea was first prepared by mixing urea with stoichiometric amount of formaldehyde solution. Ammonia solution was used to make pH at 8.5 of the mixture. The solution was kept overnight for proper digestion. Individual metal nitrates were added in such an amount with methylol urea solution in order to prepare different mole ratios of MgO: xAl_2O_3 (x is 1, 1.25, 1.5, 1.75, and 2). An additional lot of urea was further dissolved with each solution to maintain metal ion to urea to formaldehyde solution ratio as 1:2:4. HNO_3 was used to maintain the pH in acidic region. The homogeneous solution looked as transparent. It was dried on hot plate at 120°C till it becomes viscous gel. The gel becomes harder on further drying. Dried gel was ignited with a burning matchstick. The combustion reaction took place vigorously with long flame and emission of flue gases. Fluffy, porous, white and sometimes brownish coloured (due to presence of traces of carbon) powder was produced for each composition. All the powders of all compositions were subjected to heat treatment in a muffle furnace at 900°C.

2.2. Characterizations-

The morphology of powder was analyzed through field emission scanning electron microscope (FESEM, Supra 35VP Carl Zeiss, Germany). The grain details were studied via high resolution transmission electron microscopy (HETEM, TECNAI G2 30ST, FEI Company, Netherlands). The absorption spectra was obtained from UV-Visible-NIR absorption spectrometer (3600, Shimadzu, Japan) in electro-magnetic wave range of 200–2000 nm. The optical band gap energy values for magnesium aluminate spinel containing varied concentration of excess alumina (Al_2O_3) were determined through Tauc's relation [16]: $(\alpha h\nu)^n = \text{constant}(h\nu - E_g)$ where hν is the photon energy, α is the absorption coefficient, n is constant relative to the material. The dependence of the degree of absorption related to the energy of the incoming photons (hν) varies with n equals to 2 for a direct transition (E_g).

3. Results and Discussions

3.1 Morphological study of powder-

Fig. 1a-b shows the field emission scanning electron microscopic image for both x=1 & 1.75 varieties. The synthesized mass looked porous, fluffy, and loosely agglomerated. Fig. 1a indicates that the powder with x=1 composition comprises of mostly amorphous mass occasionally coexisted with very few embedded nano particles. On the other hand, alumina-richer (x=1.75) powder appeared in fully crystalline form of nearly spherical shaped nano particles (Fig. 1b). This result is the indication of emission of gaseous components in large volume, produced from combustion process that simultaneously inhibited probable sintering among particles during the exothermic combustion reactions. The observed discrepancies in development of crystallinity between different as-synthesized powders may be clarified in the light of previous investigation. Earlier literature [17] suggests that divalent cations preferentially crosslinks to the blocks of polymer gel structure in two dimensional pattern whereas the trivalent cations form stronger and stable networks with the polymer blocks in three dimensional manner. In the present case under study, gel containing stoichiometric composition of metallic ions (Mg^{2+} and Al^{3+}) dissociates into residues at comparatively much lower temperature, than the decomposition temperature of gels containing excess alumina compositions during combustion process. The comparative DTA graphs of three compositions are given in Fig. 2 in this context, which represents the dissociation temperatures of gels as 244°C for x=1.0 rose to 288°C for x=2.0. Expectedly, the low temperature exposure during cracking of gel containing stoichiometric metals- ratio is insufficient to form crystals. EDX pattern (Fig. 3) evidences well the phase purity of typical synthesized powder as the only peaks for elements like Mg, Al, and O have appeared.

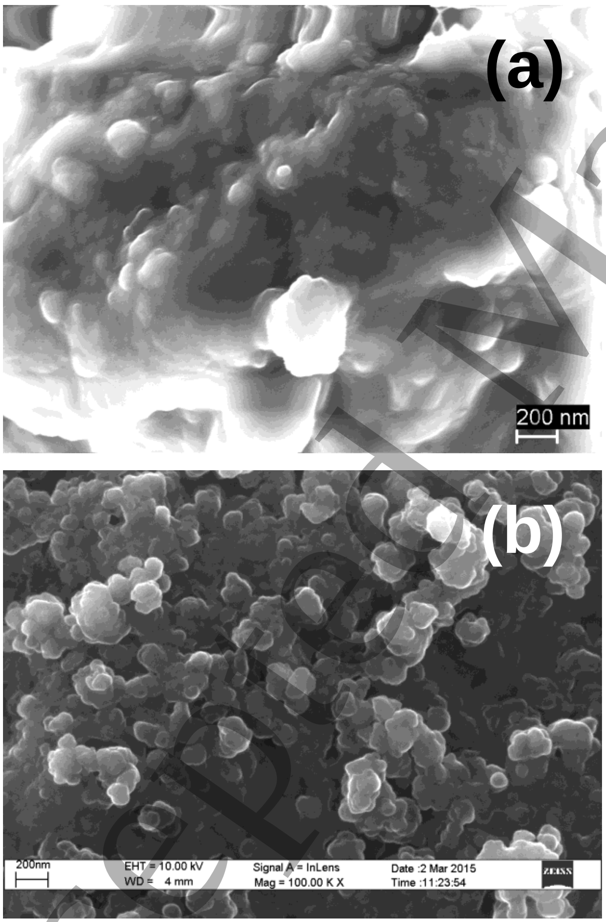

Fig. 1: FESEM micrographs for as-synthesized: (a) x=1 & (b) x=1.75 compositions.

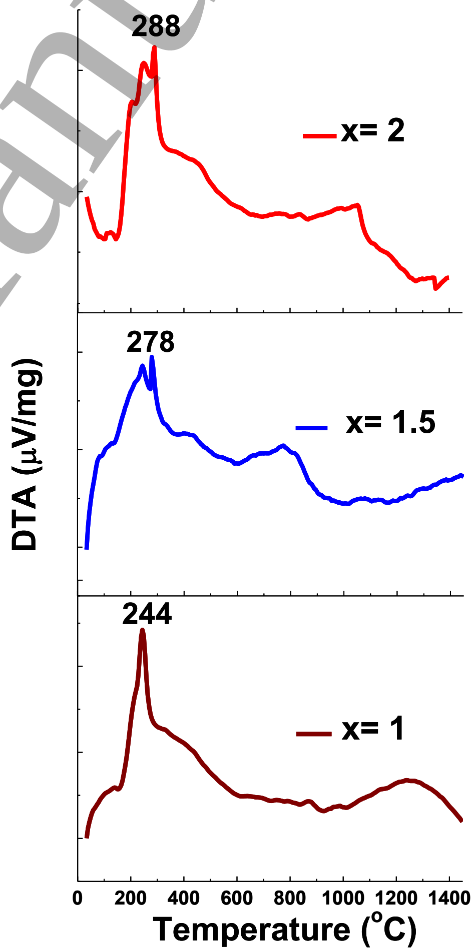

Fig. 2: Comparative study of DTA plots for dried gel containing varied trivalent to divalent cation ratio (x=1, 1.5 & 2 compositions).

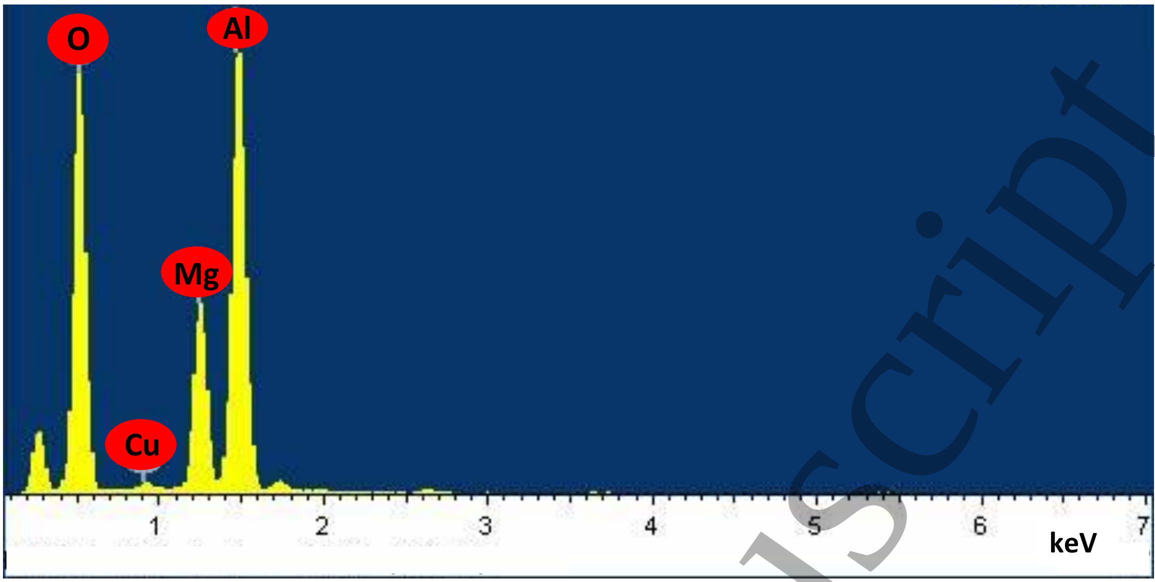

Fig. 3: EDX pattern of x=1.75 composition.

The TEM- bright field image for the post synthesis heat treated x=1 composition has been presented in Fig. 4a which reveals the fact that the larger particles are consisted of finer sized grains. A representative similar image (Fig 4b) for x=1.75 composition puts up the impression that powders from all the compositions are similarly structured. Corresponding TEM dark field image of Fig 4a is given in Fig. 4c that reveals clearer view of grain structure through strongly illuminating nano-grains of nearly spherical shape and size in the range of 10-15 nm. The observation is consistent with that of FESEM. Literature suggests that magnesium aluminate spinel powder consisting of the grains in the size range of 100-250 nm could be obtained by conventional combustion method from the solution of aluminum nitrate, magnesium nitrate and urea only [18]. Contrary to that, as obtained in the present study, comparatively much smaller crystals points out the changed role of the fuel which is a combination of formaldehyde solution and urea in otherwise same sets of reagents as used in the earlier study. The indexed SAED pattern in Fig. 4d represents the bright diffraction rings made up of the tiny bright spots those originated through the convergence of reflecting waves from different lattice planes of clustered nano-grains. Arrangement pattern of diffracting rings proves the FCC structure [19] of synthesized $MgAl_2O_4$. High resolution TEM study (as in Fig. 4e) on the individual tiny grain shows the d-spacings between the adjacent lattice fringes. Lattice fringes in the image correspond to planes (044), (335) and (155). However, one notable point worth mentioning in this section is that the trivalent to divalent cation ratio does not seem to have any observable influence on the obtained grain shapes and sizes of synthesized powders of different compositions.

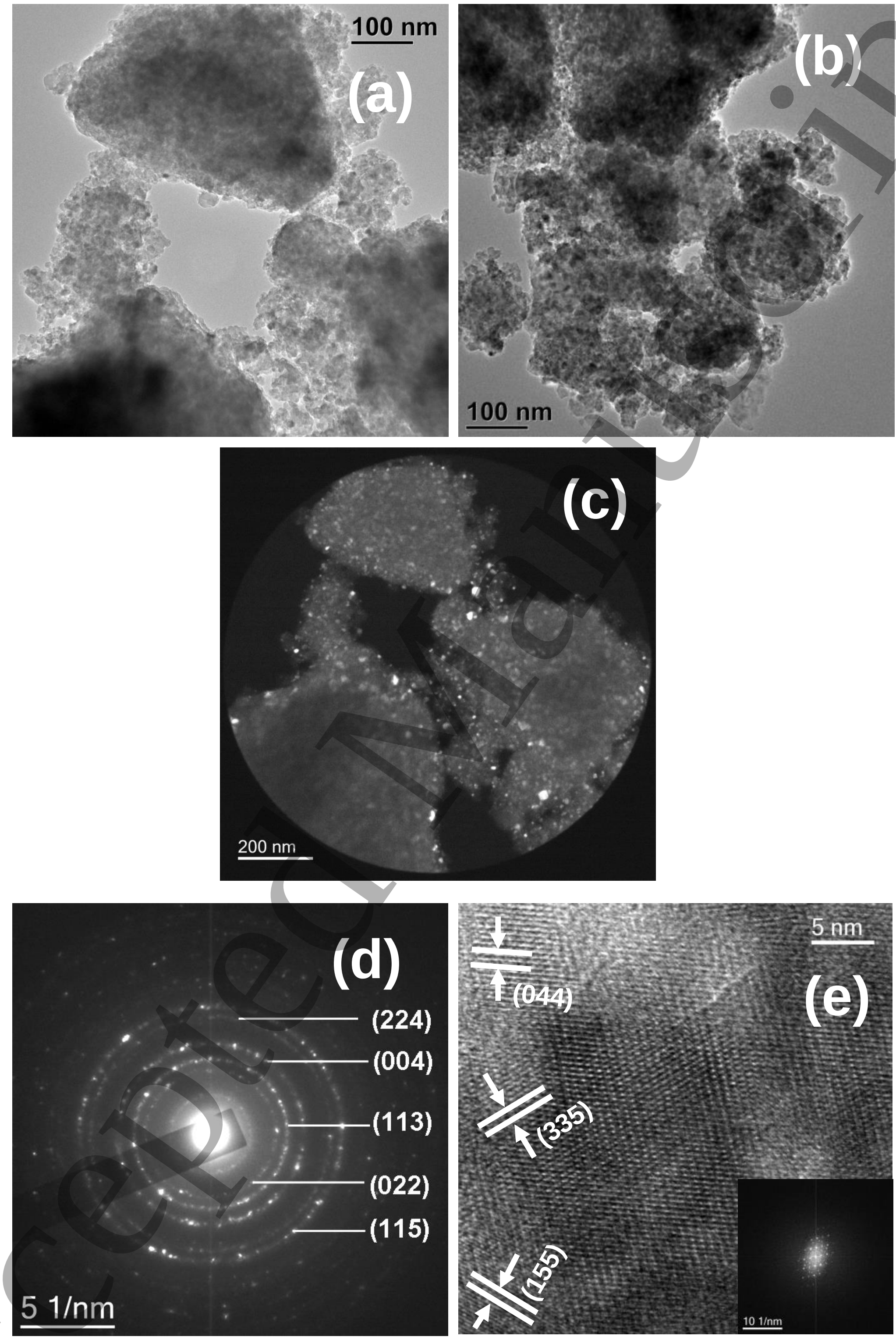

Fig. 4: TEM micrographs: (a) bright field image of x=1 composition; (b) bright field image of x=1.75 composition; (c) corresponding dark field image of Fig 4a; (d) indexed SAED pattern of x=1 composition; (e) HRTEM of x=1 composition.

3.2 Optical studies-

3.2.1 Absorbance behavior:

Influence of excess alumina on the optical property of the studied magnesium aluminate spinel powders with different values of x was investigated through the measurements of their absorption property in the UV-Vis- NIR range. Absorbance spectra as presented in Fig. 5 indicates that the powder bearing excess alumina concentrations exhibit similar absorption edge but with progressive intensity. A magnified view of increasing capability of photon absorption in the UV range of 235-335 nm (5.27–3.70 eV) has been displayed in inset of Fig. 5. The absorption intensity is highest for alumina-rich x=2 and lowest for stoichiometric x=1 compositions. Absorption peak at 284 nm (4.36 eV) may be attributed to F^+ centre electron transition [20]. This high absorption capability at UV- regime suggests that synthesized powder can be considered for photocatalytic activities [21]. No absorption peak appears in the visible wavelength regime indicating the powders to be of highly reflective nature for visible lights. Apart from this, some broad but low intensity peaks have appeared in the NIR range that substantiates absorbing capability of the powder of NIR radiations.

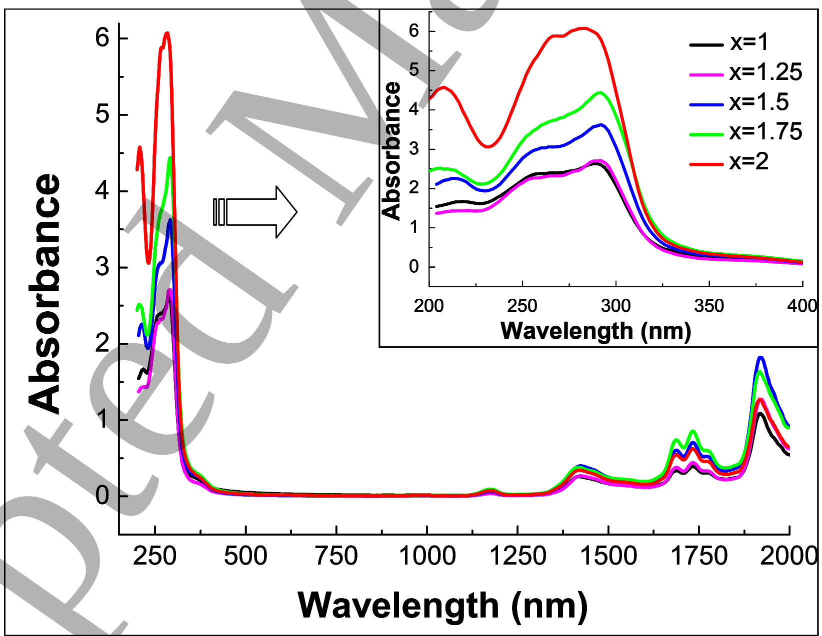

Fig. 5: Absorption spectra of different powders with compositions ranging from x=1 to 2. Enlarged view of pattern is given in inset.

3.2.2 Band gap:

Band gap values have been evaluated based upon the obtained data from the absorbance spectra of heat treated stoichiometric (x=1) as well as alumina richer compositions (x=1.25

to 2). Considering a direct band gap [22] of this material, the Tauc's plot for all compositions has been presented in Fig. 6a-e, respectively. The estimated band gap for x=1 is 3.01 eV and the value increases progressively up to 5.21 eV for x=2. The error of measurement lies within the range of ±0.077. Fig. 7 represents the estimated band gap values of concerned materials, establishing the increasing trend with increasing excess alumina concentrations. Similar result of enhancement in band gap was also found by previous researchers [21] where magnesium aluminate spinel was produced via solid state reaction method using MgO and Al_2O_3 powders. Other studies [23,24] on optical properties of the spinel oxides were done by following the First principle calculations within the generalized gradient approximation of the density functional theory while the full-potential linearized augmented plane wave method was used with the generalized gradient approximation. It was seen in case of Mg doped $ZnAl_2O_4$ system ($Mg_xZn_{1-x}Al_2O_4$) that the band gap increases from 3.851 eV to 5.079 eV with increasing doping insertion. This can be explained by the threshold of the electronic transition from O-2p to the empty Mg-3p electron states due to the substitution of Zn with Mg. Recently Tauc's relation has also been utilized in describing the change in band gap, widening followed by collapsing under high pressure compression in case of semiconductors like $InVO_4$, $InNbO_4$, and $InTaO_4$ [25].

In some of the semiconductor systems like Sn doped In_2O_3 [26] or Al doped ZnO [27] materials, increase in band gap have been observed. Following Pauli's principle for avoiding double occupation, the associated electrons of the doped ions occupy the bottom of the conduction band in a form of electron gas and block the lowest energy transitions. Due to this reason such shifting in band gap occurs, known as Burstein-Moss effect [28]. In the present study, accommodation of excess aluminium in the spinel lattice takes place by incorporation of the trivalent aluminium ions by replacing tetrahedral divalent magnesium ions [29]. Electrochemical imbalance that arises out of insertion of excess positive charge results in subsequent charge neutrality through formation of cation vacancies related to magnesium/aluminium ions as well as possible anionic vacancies. Electrical charge balance may be maintained by two ways- (1) addition of two substituting Al^{3+} ions is electrically compensated by creating vacancy of one tetrahedral Mg^{2+} ion; (2) addition of three substituting Al^{3+} ions are compensated by one of octahedral Al^{3+} ion vacancy along with one oxygen diffusion interstitials. The large trivalent cation doping in the present case could presumably simulate the situation aroused in the previous case [27] and becomes responsible for the Burstein-Moss effect to take place. The widening in band gap therefore follows the concentration of the trivalent doping.

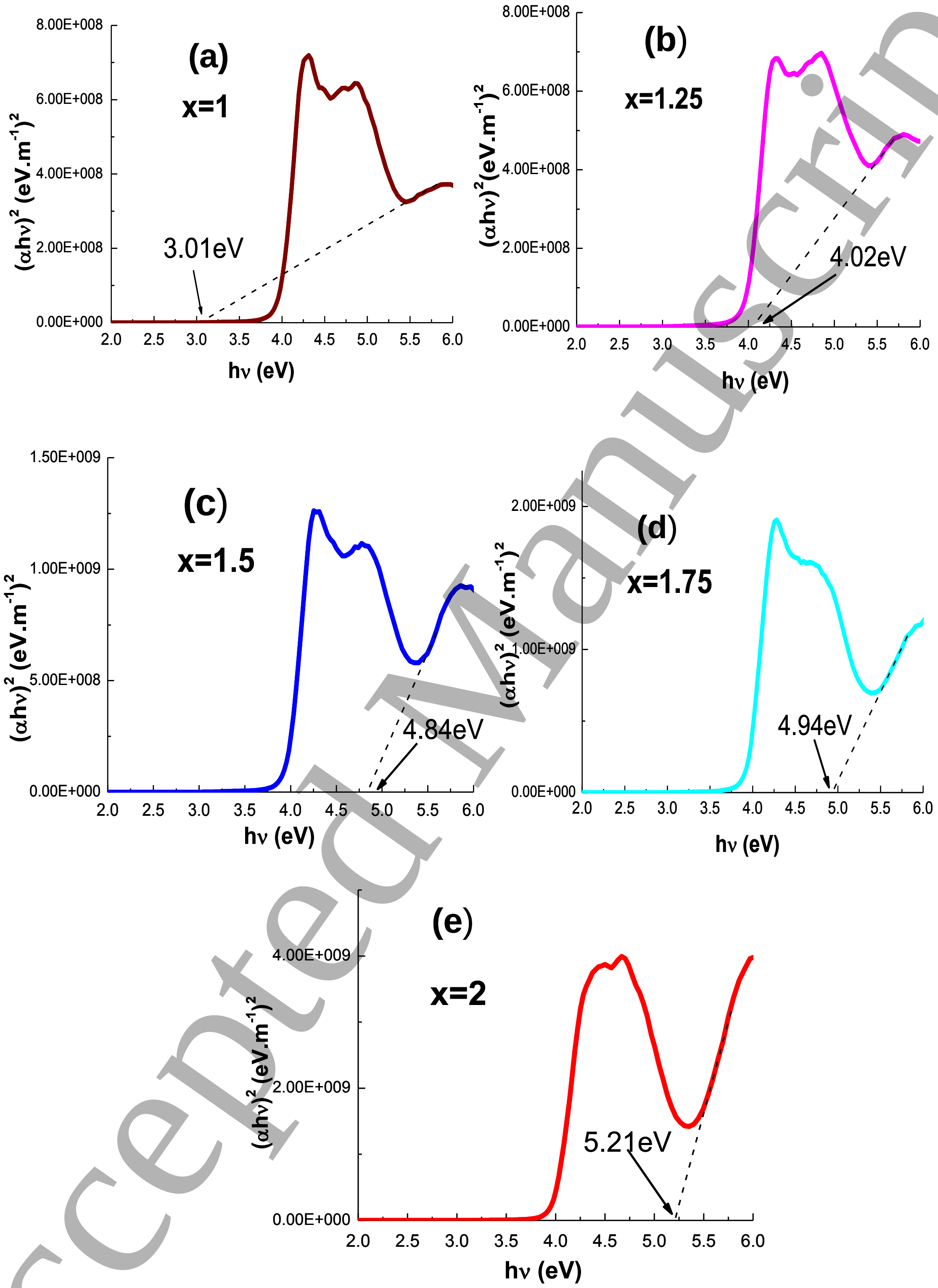

Fig. 6: Tauc's plot for, (a) x=1; (b) x=1.25; (c) x=1.5; (d) x=1.75 & (e) x=2 compositions.

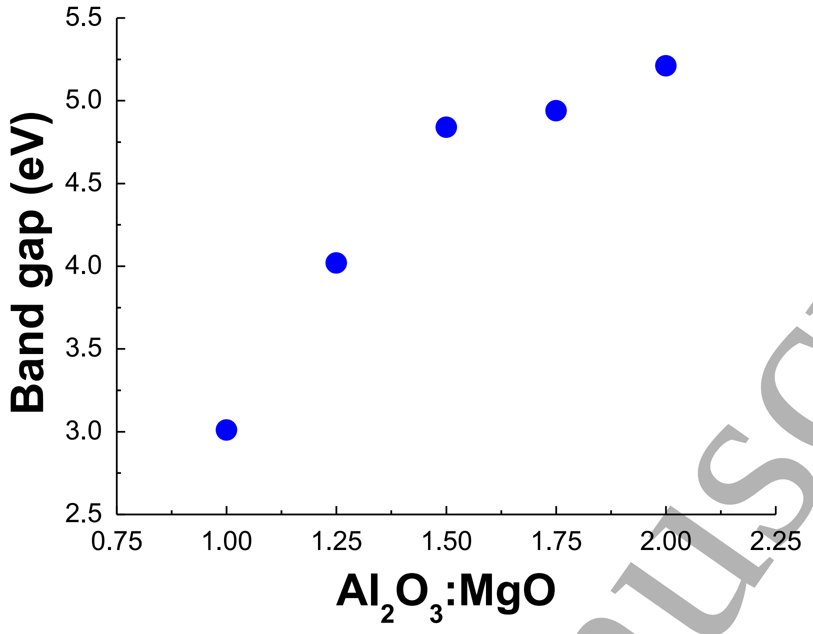

Fig. 7: Variation in band gap values against trivalent to divalent metal oxide molar ratio.

4. Conclusions

Magnesium aluminate spinel ($MgO.xAl_2O_3$) compositions along line of homogeneity with different values of x starting from 1 and ranging up to 2 were produced by urea-formaldehyde- fuelled gel combustion method. Trivalent cations, through a change in gel structure, affect the combustion temperature and subsequently the crystallinity of the produced powder. However, it does not possibly influence the grain sizes. Intensity of absorption spectra as obtained in UV- region increases with excess alumina concentration. The increase in trivalent to divalent cation ratio induces widening of energy band gap value from 3.01 eV for x=1 to 5.21 eV for x=2 compositions due to Burstein-Moss effects. Absorption study reveals that the synthesized powders are suitable for application in photocatalytic reactions.

Acknowledgements

The first author (RH) conveys sincere thanks to CSIR for Research Associate position. Helps from the institutional characterization units are gratefully acknowledged. Financial helps from CSIR project no MLP0204 is acknowledged. Thanks are due to the Director, CSIR-Central Glass & Ceramic Research Institute, for his support.

References

[1] López-Moreno S, Rodríguez-Hernández P, Muñoz A, Romero A H, Manjón F J, Errandonea D, Rusu E and Ursaki V V 2011 Lattice dynamics of $ZnAl_2O_4$ and $ZnGa_2O_4$ under high pressure *Ann. Phys.* **523** 157−167.

[2] Errandonea D, Kumar R S, Manjón F J, Ursaki V V and Rusu E V 2009 Post-spinel transformations and equation of state in $ZnGa_2O_4$: Determination at high pressure by in situ x-ray diffraction *Phys. Rev. B* **79** 024103.

[3] Catti M 2001 High-pressure stability, structure and compressibility of Cmcm-$MgAl_2O_4$: an ab initio study *Phys. Chem. Minerals* **28** 729−736.

[4] Mohapatra D and Sarkar D 2007 Preparation of MgO-$MgAl_2O_4$ composite for refractory application *J. Mater. Process. Technol.* **189** 279−283.

[5] Sharafat S, Ghoniem N M, Cooke P I H, Martin R C, Najmabadi F, Schultz K R, Wong C P C and TITAN Team 1993 Materials analysis of the TITAN-I reversed-field-pinch fusion power core *Fusion Eng. Des.* **23** 99−113.

[6] Kingery W D and Uhlmann D R 1976 Introduction to ceramics, Wiley, New York

[7] Gusmano G, Montesperelli G, Travera E and Bearzotti A 1993 Humidity-sensitive electrical properties of $MgAl_2O_4$ thin films *Sens. Actuators B* **13/14** 525– 527.

[8] Nassar M Y, Ahmed I S and Samir I 2014 A novel synthetic route for magnesium aluminate ($MgAl_2O_4$) nanoparticles using sol–gel auto combustion method and their photocatalytic properties *Spectrochim. Acta Part A: Mol. Biomol. Spectrosc.* **131** 329–334.

[9] Frage N, Cohen S, Meir S, Kalabukhov S and Dariel M P 2007 Spark plasma sintering (SPS) of transparent magnesium-aluminate spinel *J. Mater. Sci.* **42** 3273– 3275.

[10] Pei L Z, Yin W Y, Wang J F, Chen J, Fan C G and Zhang Q F 2010 Low temperature synthesis of magnesium oxide and spinel powders by a sol-gel process *Mater. Research.* **13** 339–343.

[11] Montouillout V, Massiot D, Douy A and Coutures J P 1999 Characterization of $MgAl_2O_4$ precursor powders prepared by aqueous route *J. Am. Ceram. Soc.* **82** 3299–3304.

[12] Rashad M M, Zaki Z I and Shall H E 2009 A novel approach for synthesis of nanocrystalline $MgAl_2O_4$ powders by co-precipitation method *J. Mater. Sci.* **44** 2992–2998.

[13] Bickmore C R, Waldner K F and Treadwell D R 1996 Ultrafine spinel powders by flame spray pyrolysis of a magnesium aluminum double alkoxide *J. Am. Ceram. Soc.* **79** 1419−1423.

[14] Wang C T, Lin L S and Yang S J 1992 Preparation of $MgAl_2O_4$ spinel powders via freeze-drying of alkoxide precursors *J. Am. Ceram. Soc.* **75** 2240−2243.

[15] Halder R and Bandyopadhyay S 2017 Synthesis and optical properties of anion deficient nano MgO *J. Alloys Compd.* **693** 534-542.

[16] Tauc J and Menth A 1972 States in the gap *J. Non-cryst. Solids.* **8-10** 569−585.

[17] Yang C H, Wang M X, Haider H, Yang J H, Sun J Y, Chen Y M, Zhou J and Suo Z 2013 Strengthening alginate/polyacrylamide hydrogels using various multivalent cations *ACS Appl. Mater. Interfaces* **5** 10418−10422.

[18] Ganesh I, Johnson R, Rao G V N, Mahajan Y R, Madavendra S S and Reddy B M 2005 Microwave-assisted combustion synthesis of nanocrystalline $MgAl_2O_4$ spinel powder *Ceram. Int.* **31** 67–74.

[19] Fultz B and Howe J M 2002 Transmission electron microscopy and diffractometry of materials *Springer publications, Berlin*.

[20] Jiang S, Lu T, Long Y and Chen J 2012 Ab initio many-body study of the electronic and optical properties of $MgAl_2O_4$ spinel *J. Appl. Phys.* **111** 043516.

[21] Rahman A and Jayaganthan R 2015 Study of photocatalyst magnesium aluminate spinel nanoparticles *J. Nanostruct. Chem.* **5** 147–151.

[22] Sampath S K, Kanhere D G and Pandey R 1999 Electronic structure of spinel oxides: zinc aluminate and zinc gallate *J. Phys.: Condens. Matter* **11** 3635–3644.

[23] Xiang C, Zhang J, Lu Y, Tian D and Peng C 2017 Electronic and optical properties of the spinel oxides $Mg_xZn_{1-x}Al_2O_4$ by first-principles calculations, *Mater. Technol.* **51** 735–743.

[24] Hosseini S M 2008 Structural, electronic and optical properties of spinel $MgAl_2O_4$ oxide *Phys. Status. Solidi. b* **245** 2800-2807.

[25] Botella P, Errandonea D, Garg A B, Hernandez P R, Muñoz A, Achary S N and Vomiero A 2019 High-pressure characterization of the optical and electronic properties of $InVO_4$, $InNbO_4$, and $InTaO_4$ *SN Appl. Sci.* **1** 389.

[26] Hamberg I, Granqvist C G, Berggren K F, Sernelius B E and Engstrom L 1984 Band-gap widening in heavily Sn-doped In_2O_3 *Phys. Rev. B* **30** 3240–3249.

[27] Sernelius B E, Berggren K F, Jin Z C, Hamberg I and Granqvist C G 1988 Band-gap tailoring of ZnO by means of heavy Al doping *Phys. Rev. B* **37** 10244–10248

[28] Burstein E 1954 *Phys. Rev.* **9** 632; Moss T S 1954 *Proc. Phys. Soc. London, Ser. B* **67** 775.

[29] Ting C J and Lu H 1999 Defect reactions and the controlling mechanism in the sintering of magnesium aluminate spinel *J. Am. Ceram. Soc.* **82** 841–848.